J Solid State Electrochem (2012) 16:3487–3497
DOI 10.1007/s10008-012-1800-x

ORIGINAL PAPER

Electrodeposition of nanocrystalline aluminium, copper, and copper–aluminium alloys from 1-butyl-1-methylpyrrolidinium trifluoromethylsulfonate ionic liquid

P. Giridhar · S. Zein El Abedin · F. Endres

Received: 26 April 2012 / Revised: 13 June 2012 / Accepted: 14 June 2012 / Published online: 6 July 2012

Abstract In this paper, we show that nanocrystalline aluminium, copper, and copper–aluminium alloys can be electrodeposited from the ionic liquid 1-butyl-1-methylpyrrolidinium trifluoromethylsulfonate, $[Py_{1,4}]TfO$. Furthermore, Al deposition was studied in 1-ethyl-3-methylimidazolium trifluoromethylsulfonate, [EMIm]TfO for comparison. The two employed ionic liquids exhibit different concentration-dependent phase behaviour with $AlCl_3$. This study comprises cyclic voltammetry, potentiostatic electrolysis, scanning electron microscopy, X-ray diffraction, atomic absorption spectroscopy, and inductively coupled plasma optical emission spectroscopy. Thick (in micrometre regime) and uniform layers of aluminium deposits were obtained from 2.75 M $AlCl_3$ in $[Py_{1,4}]TfO$ at 100 °C. The average crystallite size of aluminium was found to be around 40 to 50 nm. However, a coarse and cubic-shaped Al deposit with crystal sizes in the micrometre regime was obtained from [EMIm]TfO. Electrodeposition of copper was investigated in $[Py_{1,4}]TfO$-containing $Cu(TfO)_2$ at 100 °C. The average grain size of the copper deposit obtained from the electrolysis is around 20 to 40 nm. Electrodeposition of copper–aluminium alloys was successful in the same ionic liquid at 100 °C. Thick layers of copper–aluminium alloys were obtained from the employed ionic liquid. XRD analysis of the obtained deposits from electrolysis experiments revealed that Cu_3Al alloy was formed. SEM analysis indicated that the nanocrystalline copper–aluminium deposits have an average grain size of 60 to 70 nm.

Keywords Ionic liquids · Electrodeposition · Aluminium · Copper · Copper–aluminium alloy · Nanomaterials

Introduction

The electrodeposition of aluminium has been extensively reported in literature especially from ionic liquids based on organic halides and aluminium halides [1–19]. Although Lewis acidic chloroaluminate ionic liquids can be well used in the deposition of aluminium, they are quite hygroscopic. Air and moisture stable ionic liquids having 1,3-dialkylimidazolium or 1,1-dialkylpyrrolidinium cations and anions such as bis(trifluoromethylsulfonyl)amide (e.g. $[Py_{1,4}]TFSA$) have also been studied for the electrodeposition of aluminium. 1-Ethyl-3-methylimidazolium bis(trifluoromethylsulfonyl) amide ([EMIm]TFSA) and 1-butyl-1-methylpyrrolidinium bis(trifluoromethylsulfonyl)amide ($[Py_{1,4}]TFSA$) exhibit a biphasic behaviour upon the addition of $AlCl_3$ in a range of concentrations from 2.5 to 5 M and 1.6 to 2.5 M, respectively [20]. In a previous article, the characterization of the phase composition of the biphasic mixtures was described [21]. A nanocrystalline Al deposit was obtained when $[Py_{1,4}]TFSA$ was used as an electrolyte. However, a microcrystalline Al deposit was obtained in the case of [EMIm]TFSA. There is a lot of evidence that the different grain size might be due to a different adsorption of the pyrrolidinium cation on the growing nuclei and thus hindering the further growth of crystals. This assumption could be supported by studying the interface of the two ionic liquids ($[Py_{1,4}]TFSA$

For the special issue dedicated to the 75th birthday of Prof. Dr. Waldfried Plieth.

P. Giridhar · S. Zein El Abedin · F. Endres (✉)
Institute of Particle Technology,
Clausthal University of Technology,
Arnold-Sommerfeld-Strasse 6,
38678 Clausthal-Zellerfeld, Germany
e-mail: frank.endres@tu-clausthal.de

S. Zein El Abedin
Electrochemistry and Corrosion Laboratory,
National Research Centre, Dokki,
Cairo, Egypt

and [EMIm]TFSA) independently using atomic force microscopy and scanning tunnelling microscopy (STM) [22], revealing that in the neat liquid pyrrolidinium, ($[Py_{1,4}]^+$) cations interact with the substrate more strongly than $[EMIm]^+$ cations. Thus, the difference in the surface adsorption/interaction can lead to dramatic effects. Interestingly, a nanocrystalline Al deposit was also obtained from partially decomposed ionic liquids such as either [EMIm]TFSA or [EMIm]Cl/$AlCl_3$ [23]. The decomposed products of the EMIm cation seem to act as grain refiner. Unpublished in situ STM images give hints for different surface processes in comparison to the undecomposed liquids, but we have not yet got high-resolution STM images. Furthermore, a nanocrystalline Al deposit was obtained from 1-(2-methoxyethyl)-3-methylimidazolium chloride/$AlCl_3$ ([MoeMIm]Cl/$AlCl_3$) [24]. In the light of these results, we decided to study the deposition of aluminium from ionic liquids with the trifluoromethylsulfonate anion containing two different cations. So far, the electrochemical deposition of aluminium from 1-butyl-1-methylpyrrolidinium trifluoromethylsulfonate and from 1-ethyl-1-methylimidazolium trifluoromethylsulfonate ionic liquids has not yet been reported. One motivation for this study was that the electrodissolution of Cu in liquids with the TFSA anion can lead to CuF_2, a consequence of TFSA decomposition [25]. This problem is circumvented with triflate, and consequently the deposition of nanocrystalline Cu–Al Alloys becomes feasible.

Copper is an important metal and has applications in various industries including the large-scale use in electronics industry (in the production of printed circuit boards), in selective case hardening steel for engineering materials, and in printing industry [26, 27]. Copper can easily be deposited from aqueous acid solutions or from cyanide free alkaline solutions. However, these baths are highly corrosive and have several drawbacks such as the release of toxic effluents and they can pollute the environment. In this context, ionic liquids have been discussed to be potentially advantageous due to their usually negligible vapour pressure. The electrochemistry of copper and its deposition from ionic liquids containing alkylpyridinium or alkylimidazolium chlorides and $AlCl_3$ has been studied [28–30]. Several articles reported the electrodeposition of copper from air and moisture stable ionic liquids containing anions such as tetrafluoroborate [31], hexafluorophosphate [32], dicyanamide [33], trifluoromethylsulfonate [34], and bis(trifluoromethylsulfonyl)amide TFSA [35–37]. However, a breakdown of the TFSA was observed during the dissolution process of copper in $[Py_{1,4}]$TFSA [25]. Abbott's group also investigated the electrochemical deposition of copper and its composites from deep eutectic solvents based on choline chloride [38]. From a saturated solution of $Cu(TfO)_2$ in $[Py_{1,4}]$TfO, nanocrystalline Cu can be made [34].

The codeposition of metals to form alloys often leads to the reduction of the less noble metal ion at potentials more positive than predicted from thermodynamic data [39]. Brenner has classified this phenomenon as anomalous codeposition. The codeposition of certain transition elements, such as nickel [40], manganese [41], and titanium [42] with aluminium has been reported in acidic chloroaluminate alkali halide molten salts. Moffat studied the codeposition of nickel with aluminium from acidic $AlCl_3$/NaCl (2:1 mol%) and based on free energy calculations he concluded that the driving force of the codeposition process is due to an increase in free energy of the alloy formation which decreases the reduction potential of aluminium [40]. The codeposition of aluminium with some transition metals such as silver [43], nickel [44], and cobalt [45–47] has also been reported from acidic chloroaluminate ionic liquids. Furthermore, the electrochemical deposition of copper–aluminium alloys has been studied in acidic chloroaluminate ionic liquids [48, 49] leading to microcrystalline deposits. Hitherto, there is no report available on the electrochemical deposition of copper–aluminium alloys from air and moisture stable ionic liquids such as 1-butyl-1-methylpyrrolidinium trifluoromethylsulfonate.

Experimental

The ionic liquids, 1-butyl-1-methylpyrrolidinium trifluoromethylsulfonate, ($[Py_{1,4}]$TfO), 1-ethyl-3-methylimidazolium trifluoromethylsulfonate, ([EMIm]TfO), were purchased from IOLITEC, GmbH, Germany. The quality of the ionic liquids given by the supplier is 99 %. The water content of the as received ionic liquids $[Py_{1,4}]$TfO and [EMIm]TfO was found to be 341 and 117 ppm, respectively (Karl Fischer Titration). Furthermore, the liquids can contain trifluoromethylsulfonic acid in the ~100-ppm regime. Aluminium chloride grains (>99 %) were purchased from Fluka, and Cu(II) trifluoromethylsulfonate ($Cu(TfO)_2$; 99 %) was purchased from Aldrich. Gold substrates (gold films of 200–300 nm thickness deposited on chromium-covered borosilicate glass) were procured from Arrandee Inc.

The ionic liquids were further dried for 2 days at 373 K under vacuum and stored in closed bottles in an argon-filled glove box. The water and oxygen contents in the glove box are below 2 ppm (Omnilab from vacuum atmospheres). The water content of the dried ionic liquids $[Py_{1,4}]$TfO and [EMIm]TfO was determined by Karl Fischer titration (4 and 7 ppm, respectively). Various concentrations of $AlCl_3$ (1.6, 2.0, 2.5, and 2.75 M) in $[Py_{1,4}]$TfO were prepared and used for the electrochemical experiments. For the deposition experiments of Al, a concentration of 2.75 M $AlCl_3$ was used. Several concentrations of $AlCl_3$ (from 1.6 to 5.0 M) in [EMIm]TfO were also prepared. A concentration of 4.6 M $AlCl_3$ was utilised for the deposition of Al from [EMIm]TfO. Two different concentrations of 0.01 and 0.025 M $Cu(TfO)_2$ in $[Py_{1,4}]$TfO were used to study the electrodeposition of

copper on gold at 100 °C. Pt wires were used as quasi reference and counter electrodes and for copper deposition experiments, copper sheets were used as counter electrodes. For copper–aluminium studies, a solution with concentrations of 2.75 M $AlCl_3$ and 0.025 M $Cu(TfO)_2$ in $[Py_{1,4}]TfO$ was prepared and used for electrochemical experiments. Cu wires and Cu sheets were used as reference electrode and counter electrodes, respectively. All experiments were carried out at 100 °C as the $AlCl_3$-containing liquids are quite viscous near room temperature. Electrochemical measurements were carried out using a PARSTAT 2263 potentiostat/galvanostat controlled by PowerCV software. Cyclic voltammograms have been recorded using a three-electrode cell. Prior to use, gold working electrodes were annealed in a hydrogen flame to red glow for a few minutes. A constant potential was applied for the electrolysis experiments, either gold or mild steel were used as working electrodes. A high-resolution SEM (Carl Zeiss DSM 982 Gemini) was employed to investigate the surface morphology of the deposited films. X-ray diffraction patterns were recorded at room temperature using a Siemens D-5000 diffractometer with CoK_α radiation at room temperature. Elemental analysis of the deposits was carried out using Atomic Absorption Spectroscopy (for copper analysis, PU 9200 Pye Unicam, Philips Inc.) and inductively coupled plasma optical emission spectroscopy (for aluminium analysis, Spectro Flame, Modula 2000, Spectro Firm).

Results and discussion

The electrochemical window of the neat ionic liquid, $[Py_{1,4}]TfO$ was found to be 5.75 V at room temperature. It is observed from Fig. 1 that the onset of cation reduction (at c_1) and anion oxidation (at a_3) are observed at −3.25 and 2.5 V, respectively. If the switching potential is set below −3.0 V, two more oxidation waves were observed at a_1 and a_2 and these were attributed to the oxidation of cation decomposition products.

The electrochemical window of the neat ionic liquid $[Py_{1,4}]TfO$ was found to be only 4.75 V at 100 °C. Figure 2 shows that the onset of the irreversible reduction of the cation and the oxidation of the anion occur at −2.75 and at 2.0 V, respectively. Two reduction waves were also observed at around −0.5 and −1.2 V and these can be attributed either to a low amount of impurities that are present in the ionic liquid or to an adsorption of ionic liquid on gold. The narrowing of the electrochemical window with increasing temperature nicely shows that there are also kinetic phenomena that determine the electrochemical window.

Electrodeposition of aluminium from $[Py_{1,4}]TfO$

In preliminary experiments, a concentration of 1.6 M $AlCl_3$ was prepared by adding an appropriate amount of $AlCl_3$ to $[Py_{1,4}]TfO$. A clear solution was obtained in the beginning and slowly transforming completely to a white solid phase. In the case of $AlCl_3/[Py_{1,4}]TFSA$, a solidification occurred at a concentration of 2.7 M $AlCl_3$ [50, 51]. Here, solidification was already observed at a concentration of 1.6 M in the case of $[Py_{1,4}]TfO$. Upon heating to above 80 °C, a colourless solution was obtained again. This behaviour is in contrast to the biphasic behaviour of $AlCl_3$ in $[Py_{1,4}]TFSA$, where a turbid and more viscous upper phase and a colourless, clear lower phase were observed [49]. The comparison of cyclic voltammograms at different concentrations of $AlCl_3$ recorded on gold is depicted in Fig. 3. At concentrations below 2.5 M $AlCl_3$ in $[Py_{1,4}]TfO$, the onset of reduction was observed at E=−1.85 V, whereas for C>2.5 M $AlCl_3$ in $[Py_{1,4}]TfO$, the onset was at −1.7 V indicating that the Al

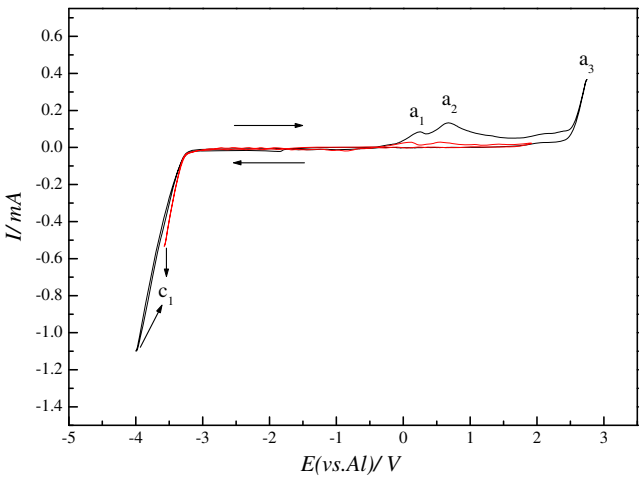

Fig. 1 Cyclic voltammogram of neat $[Py_{1,4}]TfO$ ionic liquid on gold at room temperature. Scan rate=10 mVs^{-1}

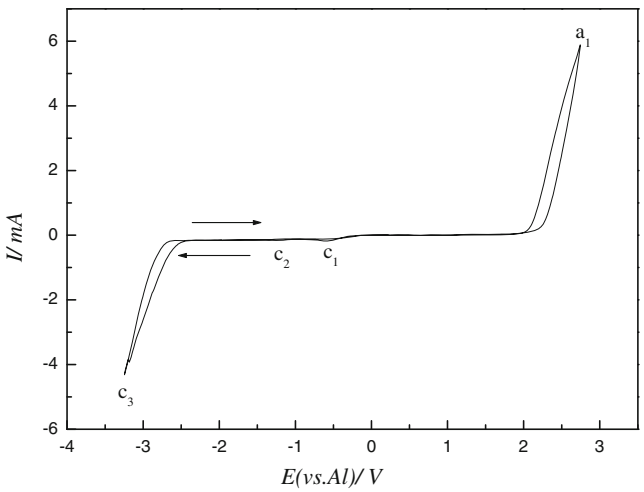

Fig. 2 Cyclic voltammogram of neat $[Py_{1,4}]TfO$ ionic liquid on gold at 100 °C. Scan rate=10 mVs^{-1}

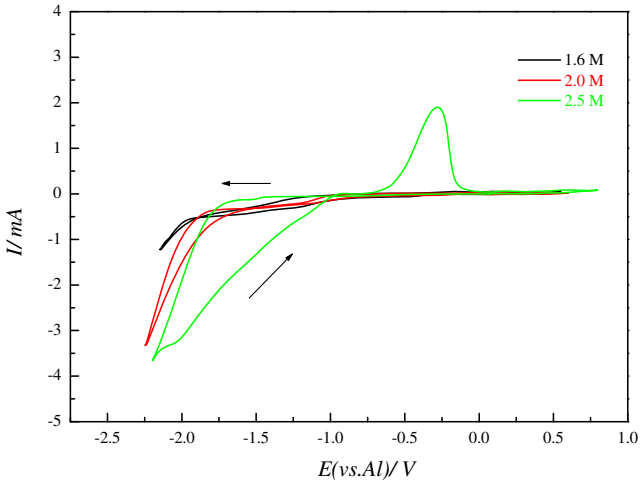

Fig. 3 Comparison of cyclic voltammograms at various concentrations of $AlCl_3$ in $[Py_{1,4}]TfO$ on gold at 100 °C. Scan rate=10 mVs^{-1}

species is subject to a different complexation. Furthermore, no Al stripping peaks were observed for concentrations below 2.5 M $AlCl_3$ in $[Py_{1,4}]TfO$. However, an oxidation wave (at + 0.75 V) was observed in the case of 2.5 M $AlCl_3$ in $[Py_{1,4}]TfO$. Thus, in subsequent experiments, the concentration of $AlCl_3$ was further increased from 2.5 to 2.75 M and cyclic voltammograms were recorded. We can conclude from this concentration dependence that only at C>2.5 M reducible Al species exist in the solution. It is worth noting that the phase behaviour and aluminium speciation in the TFSA-based ionic liquids was studied experimentally and theoretically by several groups [50–52]. Eiden et al. studied the speciation of Al in two different ionic liquids, namely $[Py_{1,4}]TFSA$ and [EMIm]TFSA, using multinuclear NMR spectroscopy and Raman spectroscopy [50]. It was stated that the Al deposition occurs in the upper phase from a four coordinated $[AlCl_2(TFSA)_2]^-$ species. Al speciation in ionic liquids, $[Py_{1,4}]TFSA$ and 1-propyl-1-methylpiperidinium bis(trifluoromethylsulfonyl) amide ($[C_3mpip][TFSA]$), was also reported by T. Rodopoulos et al. using electrochemical and variable temperature NMR spectroscopy [52]. They reported that the electrodeposition of Al occurs from the electroactive species such as $[AlCl_3(TFSA)]^-$ and $[AlCl_2(TFSA)_2]^-$. Furthermore, they reported Al electrodeposition is also possible from a six coordinated $[AlCl_2(TFSA)_2]^-$ at slightly higher temperatures at significantly lower concentrations of $AlCl_3$. Rocher et al [51] also reported the Al electrochemistry, phase behaviour and speciation in $[Py_{1,4}]TFSA$ using NMR spectroscopy (^{27}Al and ^{19}F), Raman spectroscopy, and DFT theoretical calculations. The possible electroactive species that are responsible for Al electrodeposition are $AlCl_3(TFSA)]^-$ and $[AlCl_2(TFSA)_2]^-$. Thus, it can be concluded that Al speciation might play an important role in Al electrodeposition from the triflate-based ionic liquid. Spectroscopy techniques such as NMR (^{27}Al and ^{19}F) and Raman may be useful to understand the Al speciation/complexation in $[Py_{1,4}]TfO$ ionic liquid.

In the case of 2.75 M $AlCl_3$ in $[Py_{1,4}]TfO$, the onset of Al deposition was found to be around −0.8 V, and this positive shift in reduction potential of Al^{3+} species is a clear evidence of reducible electroactive species, leading to the bulk deposition of metallic Al. Figure 4 shows a comparison of the cyclic voltammograms of 2.75 M $AlCl_3$ at two different switching potentials recorded on gold. A reduction wave was observed due to bulk deposition of Al and the corresponding stripping peak was observed at 0.25 V. There were no hints for underpotential deposition processes in the cyclic voltammograms. The cyclic voltammograms exhibit the same features and a slight positive shift in the oxidation peak potential was observed when the switching potential was varied. A loop was observed upon the scan reversal at the cathodic limit indicating nucleation processes, associated with an overpotential to induce the nucleation and growth of aluminium on the foreign substrate.

Since electroplating of aluminium on mild steel is of significant interest due to the protection of mild steel against corrosion, the electrodeposition of Al was also studied using mild steel as a working electrode. The inset of Fig. 4 represents the comparison of CVs at two different switching potentials from 2.75 M $AlCl_3$ in $[Py_{1,4}]TfO$. A nucleation loop was also observed during scan reversal. Potentiostatic electrolysis was carried out to deposit Al from 2.75 M $AlCl_3$ in $[Py_{1,4}]TfO$ at two different applied potentials, −1.0 and −1.25 V for 1 h either on gold or on mild steel substrates. The obtained deposits were washed with isopropanol followed by water and then analysed by high-resolution scanning electron microscopy and X-ray diffraction. Thick and smooth Al deposits were obtained on either gold or on mild

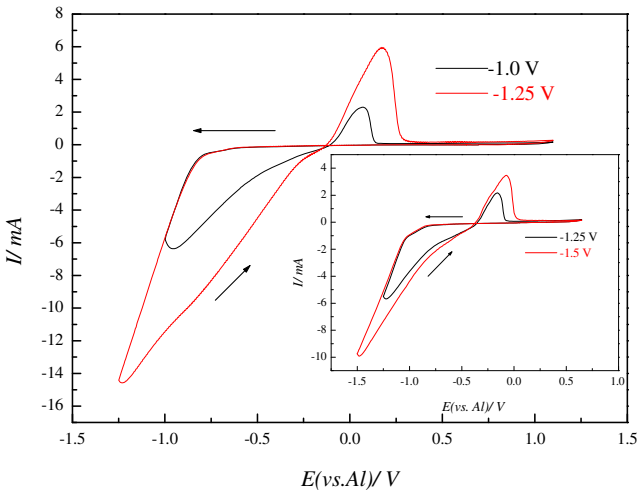

Fig. 4 Comparison of cyclic voltammograms of 2.75 M $AlCl_3$ in $[Py_{1,4}]TfO$ on gold at a scan rate of 10 mVs^{-1} at 100 °C. *Inset*: comparison of cyclic voltammograms of 2.75 M $AlCl_3$ in $[Py_{1,4}]TfO$ on mild steel at a scan rate of 10 mVs^{-1} at 100 °C

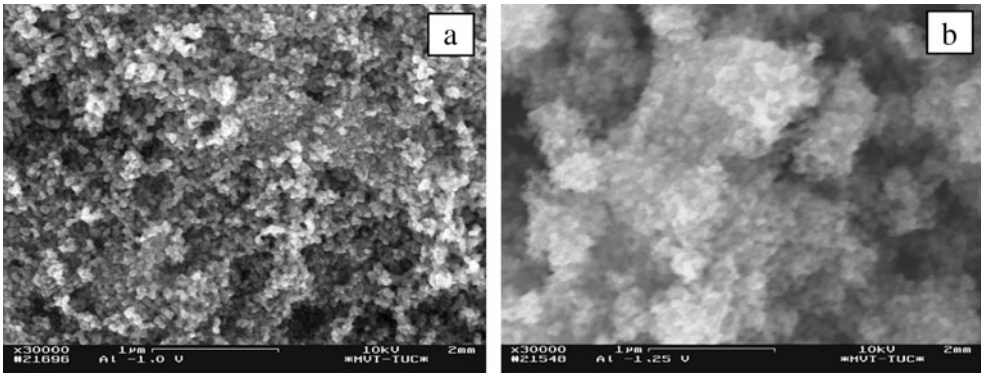

Fig. 5 SEM micrographs of as deposited aluminium on gold after electrolysis of 2.75 M $AlCl_3$ in $[Py_{1,4}]TfO$ for 1 h at two different applied potentials at 100 °C

steel. Figure 5 represents the SEM images of Al deposits on gold at the applied potentials of −1.0 and −1.25 V for 1 h at 100 °C. Uniform deposits were obtained with very fine crystallite sizes in the nanometre regime (40 to 50 nm). It was supposed that the $[Py_{1,4}]^+$ cation acts as a grain refiner due to its adsorption on the growing nuclei preventing their further growth. The assumption was already verified in the case of electrodeposition of Al from the ionic liquid $[Py_{1,4}]$TFSA containing 1.6 M $AlCl_3$. This finding was also verified by preparing various compositions of [EMIm]Cl/$AlCl_3$ (40/60 mol%) and $[Py_{1,4}]Cl/AlCl_3$ (40/60 mol%), and we obtained nanocrystalline Al deposits from the mixture of ionic liquids (at and above 80:20 vol% of $[Py_{1,4}]Cl/AlCl_3$/[EMIm]Cl/$AlCl_3$) [53].

For XRD analysis, Al was deposited on mild steel under the same conditions reported for gold. The XRD patterns of electrodeposited Al at −1.0 and −1.25 V on mild steel for 1 h at 100 °C are shown in Fig. 6. As seen from the figure, the deposited Al is crystalline and a strong diffraction peak (200) is obtained along with the other characteristic diffraction peaks (111), (220), (311), and (222). Furthermore, the diffraction peaks are broad indicating the small crystal size of the Al deposit. The average crystal size could be determined by the Scherrer equation [54] and the average size was found to be about 50 nm, which is in good agreement with the SEM result. Figure 6 also shows the XRD patterns of Al electrodeposited on mild steel from the upper phase of 4.6 M $AlCl_3$ in [EMIm]TfO and will be discussed later.

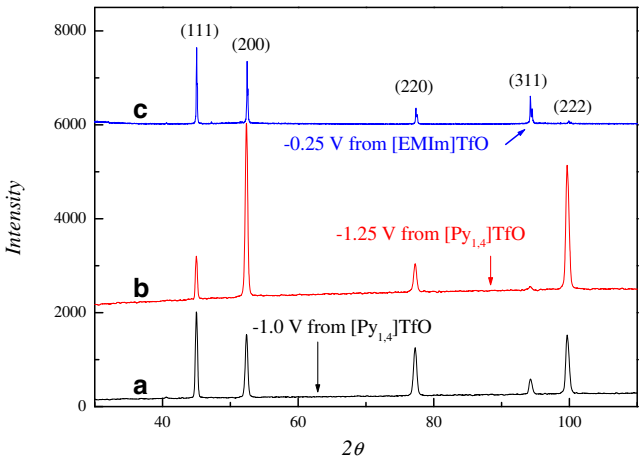

Fig. 6 XRD patterns (Co K_α) of electrodeposited Al on mild steel; **a**–**b** from 2.75 M $AlCl_3$ in $[Py_{1,4}]TfO$ at two different potentials for 1 h at 100 °C; **c** from the upper phase of 4.6 M $AlCl_3$ in [EMIm]TfO at −0.25 V for 1 h at 100 °C

Electrodeposition of aluminium from [EMIm]TfO

The electrochemical window of the neat ionic liquid, [EMIm]TfO, was found to be 4.05 V at room temperature. It is observed from Fig. 7 that the onset of cation reduction (at c_2) and anion oxidation (at a_4) are observed at ~−2.15 and ~+1.9 V, respectively. If the switching potential is set below −3.0 V, three oxidation waves were also observed at a_1, a_2, and a_3, and these were attributed to the oxidation of cation decomposition products. The reduction process at c_1 might be attributed either to adsorption of the ionic liquid on gold or to the impurities of the ionic liquid. It is worthwhile to mention the decomposition of ionic liquids by

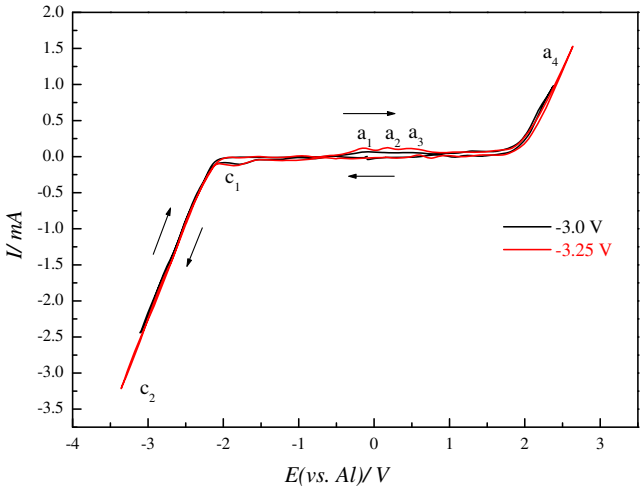

Fig. 7 Cyclic Voltammogram of neat [EMIm]TfO ionic liquid on gold at room temperature. Scan rate=10 mVs^{-1}

electrochemical means. The electrochemical breakdown of ionic liquids, $[Py_{1,4}]TFSA$ and $[BMIm]BF_4$, in the cathodic regime at higher applied voltages (8 V) was experimentally studied and theoretically predicted by M. C. Kroon et al. In the case of [Py1,4]TFSA, the decomposed products were found and verified to be as methylpyrrolidine, octanes, octenes, 2-butanol, dibutylmethylamine, and butylpyrrolidine [55].

The electrochemical window of the neat ionic liquid [EMIm]TfO was found to be only 3.6 V at 100 °C. It is observed from Fig. 8 that the onset of the irreversible reduction of the cation and the oxidation of the anion is found at ~−1.9 and ~+1.7 V, respectively. Two reduction waves were also observed at around −0.15 and −1.7 V and these were attributed either to impurities that are present in the ionic liquid or to the adsorption of ionic liquid on gold. Furthermore, two oxidation waves are observed at a_1 and a_2, these are correlated to the cation decomposition products. The narrowing of the electrochemical window with increasing temperature indicates for this liquid, too, that there are also kinetic processes determining the electrochemical window of an ionic liquid.

In initial experiments, a concentration of 1.6 M $AlCl_3$ was prepared by adding an appropriate amount of $AlCl_3$ to [EMIm]TfO (the desired amount of $AlCl_3$ was added in small quantities). A clear solution was obtained. However, no deposition of Al was observed from this solution. In subsequent experiments, the concentration of $AlCl_3$ was increased from 1.6 to 3.75 M. The prepared solutions were allowed to stand for more than 2 days to see whether it leads to the formation of a biphasic mixture or not. Clear and pale yellow solutions were obtained below 3.0 M concentration of $AlCl_3$. However, a biphasic mixture was obtained from 3.0 to 4.25 M concentration of $AlCl_3$ in the ionic liquid, and the volume of the lower phase increased with an increase in $AlCl_3$ concentration. A clear, more viscous, and light yellow upper phase and a gel-type lower phase were obtained in this range of $AlCl_3$ concentration. Furthermore, the viscosity of the upper phase increased with the increase in $AlCl_3$ concentration from 3.0 to 4.25 M in the ionic liquid, as seen by the naked eye.

Electrodeposition experiments were carried out for the solutions in the range of $AlCl_3$ concentration from 3.0 to 4.25 M, and we could not obtain a bulk deposit from this range of $AlCl_3$ concentration, rather a very thin and mirror-like film of Al was obtained. Further experiments were carried out by increasing the concentration to 4.5 M and above. Upon increasing the concentration of $AlCl_3$ from 4.25 to 4.5 M and above, a biphasic mixture was formed after allowing the solution to settle for more than 2 days. In this range of $AlCl_3$ concentration, also a clear, less viscous, and pale yellowish brown upper phase and a solid lower phase were observed. Apparently the viscosity of the upper phase of 4.6 M $AlCl_3$ is lower than the viscosity of upper phase of 4.25 M $AlCl_3$ from visual inspection. However, in this concentration regime, the volume of the upper phase increased compared to the volume of the upper phase at 4.25 M (the lower phase is a gel type at and below 4.25 M). A complete solidification was observed at and above a concentration of 4.75 M $AlCl_3$ in the employed ionic liquid.

At this juncture, it is worth comparing the phase behaviour of $AlCl_3$ in [EMIm]TFSA and [EMIm]TfO ionic liquids. In the case of $AlCl_3$/[EMIm]TFSA, a biphasic behaviour was observed in the range of $AlCl_3$ concentration from 2.5 to 5 M. This biphasic behaviour of $AlCl_3$ in [EMIm]TFSA (where a turbid and more viscous lower phase and a colourless, clear upper phase were observed) is in contrast to the $AlCl_3$ in [EMIm]TfO [49]. Furthermore a solidification of the lower phase was observed above 5.0 M $AlCl_3$ in [EMIm]TFSA,

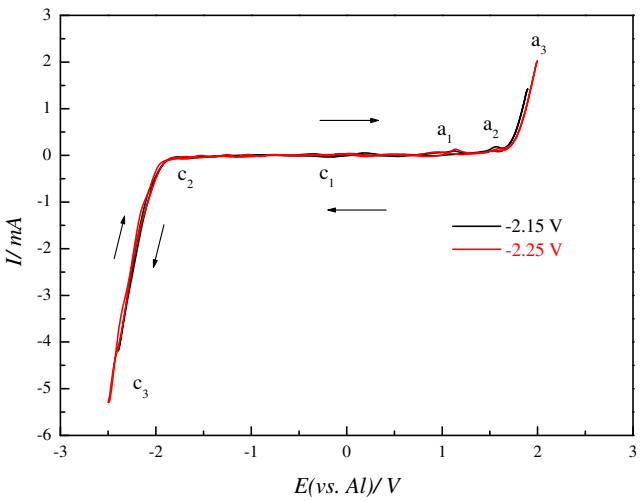

Fig. 8 Cyclic voltammogram of neat [EMIm]TfO ionic liquid on gold at 100 °C. Scan rate=10 mVs^{-1}

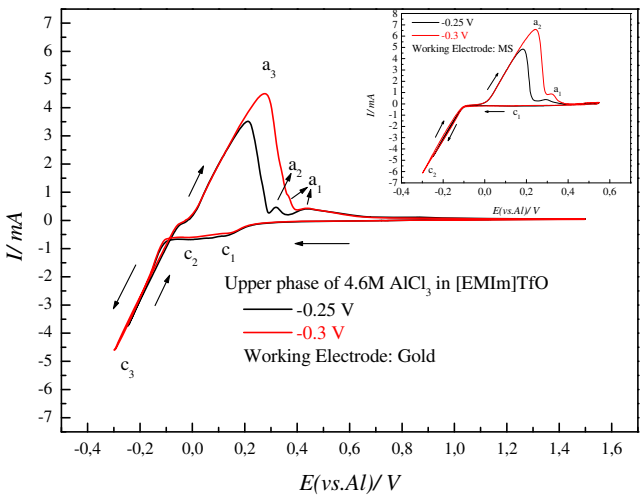

Fig. 9 Comparison of cyclic voltammograms of upper phase of 4.6 M $AlCl_3$ in [EMIm]TfO on gold at a scan rate of 10 mVs^{-1} at 100 °C. *Inset*: comparison of cyclic voltammograms of upper phase of 4.6 M $AlCl_3$ in [EMIm]TfO on mild steel at 100 °C. Scan rate: 10 mVs^{-1}

whereas a complete solidification was observed at a concentration 4.75 M $AlCl_3$ in the case of [EMIm]TfO.

The cyclic voltammograms of the upper phase of the biphasic mixture of 4.6 M $AlCl_3$ on gold at 100 °C are shown in Fig. 9. Unlike in the case of Al deposition from $[Py_{1,4}]$TfO, two reduction processes (c_1 and c_2) were observed prior to the bulk deposition of Al (c_3). The onset of Al deposition was found to be at −0.1 V (vs. Al) and the corresponding oxidation wave was observed with a peak potential at ~0.21 V. In the backward scan, two oxidation processes were observed at a_1 and a_2 and these are correlated to the reduction processes at c_1 and c_2, respectively. The electrode potential was set at −0.25 V for a few minutes to deposit aluminium from the upper phase of 4.6 M $AlCl_3$/[EMIm]TfO. Thick layers of Al were observed on the working electrode surface. This indicates that the reducible Al species are present only in the upper phase, leading to bulk Al deposits. Furthermore, a lower nucleation overpotential is observed in the case of Al deposition from [EMIm]TfO (~20 mV) when compared to the Al deposition from $[Py_{1,4}]$TfO (>−0.55 V). The inset of Fig. 9 represents the comparison of CVs recorded on mild steel at two different switching potentials from the upper phase of 4.6 M $AlCl_3$ in [EMIm]TfO at 100 °C. These voltammograms also exhibit similar features to that of the CVs recorded on gold except the reduction processes at c_1 and c_2, supporting the assumption of Al underpotential deposition (UPD) on gold.

Potentiostatic electrolysis was carried out to deposit Al from the upper phase of 4.6 M $AlCl_3$ in [EMIm]TfO at an applied potential of −0.25 V for 1 h either on gold or on mild steel substrates. The obtained deposits were washed thoroughly in a stream of isopropanol followed by water and then analysed by high-resolution scanning electron microscopy. Thick and smooth Al deposits were obtained on either gold or on mild steel. Figure 10 represents the SEM images of Al deposits on gold at the applied potentials of −0.25 V for 1 h at 100 °C. A uniform deposit was obtained with crystal sizes in the micrometre regime. As seen from the Fig. 10, the deposit is compact, dense, and consists of cubical-shaped coarse crystals.

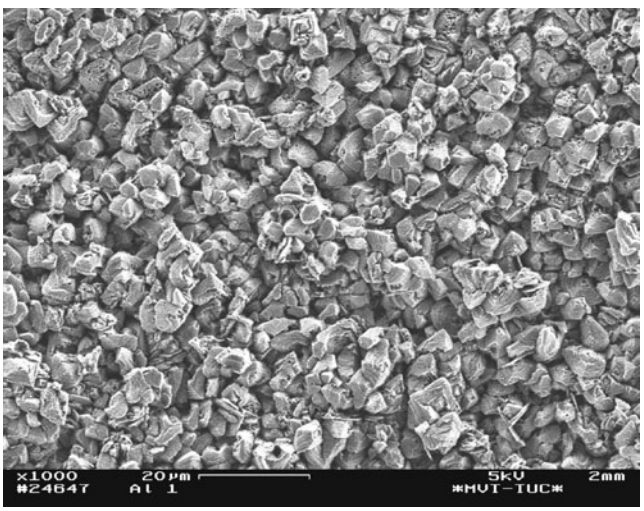

Fig. 10 SEM micrographs of as deposited aluminium on gold after electrolysis of upper phase of 4.6 M $AlCl_3$ in [EMIm]TfO for an hour at an applied potential of −0.25 V at 100 °C

For XRD analysis, Al was deposited on mild steel under the same conditions reported for gold. The XRD patterns of electrodeposited Al at −0.25 V on mild steel for 1 h at 100 °C are shown in Fig. 6. As seen from the figure, the deposited Al is crystalline and a strong diffraction peak (111) is obtained in addition to the other characteristic diffraction peaks (200), (220), (311), and (222). Furthermore, the diffraction peaks are narrow indicating the large crystal size of the Al deposit.

From the aforementioned results and discussion it can be concluded that the concentration-dependent phase behaviour of $AlCl_3$ is different in the employed TfO ionic liquids, where a complete solidification is observed at a concentration of 1.6 M $AlCl_3$ in $[Py_{1,4}]$TfO and a complete solidification is observed at and above a concentration of 4.75 M $AlCl_3$ in the case of [EMIm]TfO. Furthermore, a nanocrystalline Al deposit was obtained from the ionic liquid $[Py_{1,4}]$TfO, whereas a microcrystalline Al deposit was obtained from [EMIm]TfO ionic liquid.

Electrodeposition of copper

The cyclic voltammogram of 0.01 M $Cu(TfO)_2$ in $[Py_{1,4}]$TfO on gold at 100 °C is shown in Fig. 11. The electrode potential was scanned intially from the open circuit potential (~0.008 V) to negative direction. In the forward scan, two reduction processes (c_1 and c_2) are observed. The reduction wave at c_1 can be attributed to reduction of Cu(II) to Cu(I),

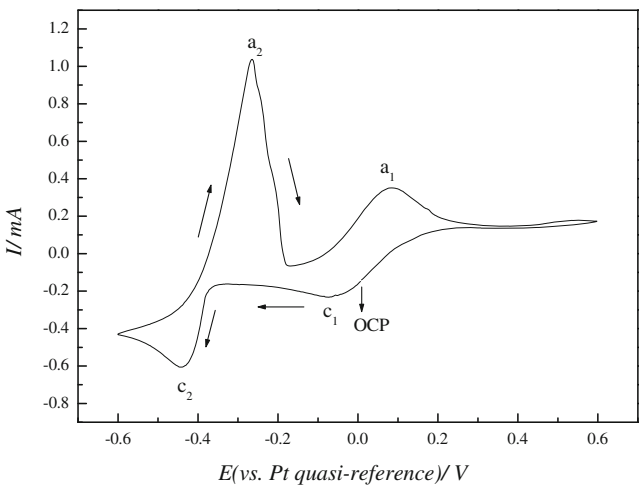

Fig. 11 Cyclic voltammogram of 0.01 M $Cu(TfO)_2$ in $[Py_{1,4}]$TfO at a scan rate of 10 mVs^{-1} on gold at 100 °C. Scan rate=10 mVs^{-1}

and the reduction wave at c_2 is clearly due to the bulk deposition of copper. A similar electrochemical behaviour was also observed in the case of $Cu(TFSA)_2$ in [THMA] TFSA by Murase et al. [35].

In order to confirm the above-observed behaviour, the solution was electrolysed by holding the electrode potential at −0.2 V for 30 min and no deposit was observed on the working electrode, this indicates that the reduction process is due to the reduction of Cu(II) to Cu(I). A controlled potential electrolysis was carried out to deposit copper from a solution of 0.025 M $Cu(TfO)_2$ in $[Py_{1,4}]TfO$ at −0.6 V on gold for 1 h at 100 °C. The obtained deposits were thoroughly washed with isopropanol followed by water to remove traces of the ionic liquid. The washed sample was analysed by high-resolution scanning electron microscopy and X-ray diffraction. A thick and uniform deposit was obtained with very fine crystal sizes (~20 to 40 nm) at −0.6 V and the corresponding SEM micrograph is shown in Fig. 12.

For XRD analysis, copper was deposited on mild steel under the same experimental conditions reported for gold. The X-ray diffraction patterns of electrodeposited copper at two different potentials, −0.5 V and −0.6 V on mild steel for 1 h are shown in Fig. 13. It can be seen from the figure that the deposited copper is crystalline and a strong diffraction peak (111) is obtained along with the other characteristic diffraction peaks (200), and (220). Furthermore, the diffraction peaks are sharp and broad indicating the small crystal size of the copper deposit. The average crystal size could be determined by the Scherrer equation [54], and it was found to be about 45 nm, which is more or less in agreement with the SEM results.

Electrodeposition of copper–aluminium alloys

$Cu(TfO)_2$ and $AlCl_3$ were used as sources of Cu(II) and Al(III) ions for the deposition experiments. A solution of

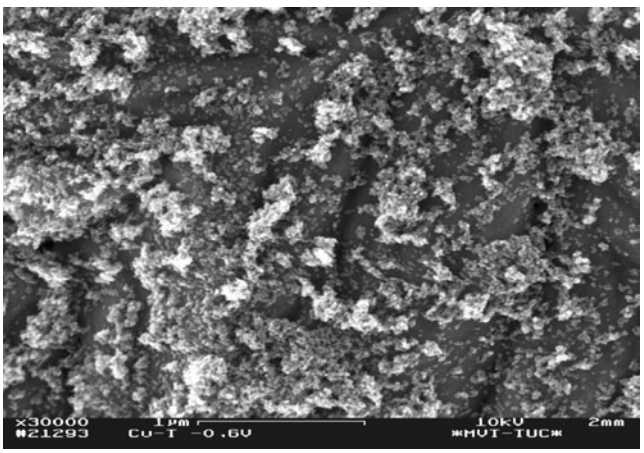

Fig. 12 SEM micrograph of as deposited Cu on gold from 0.025 M $Cu(TfO)_2$ in $[Py_{1,4}]TfO$ at −0.6 V at 100 °C for 1 h

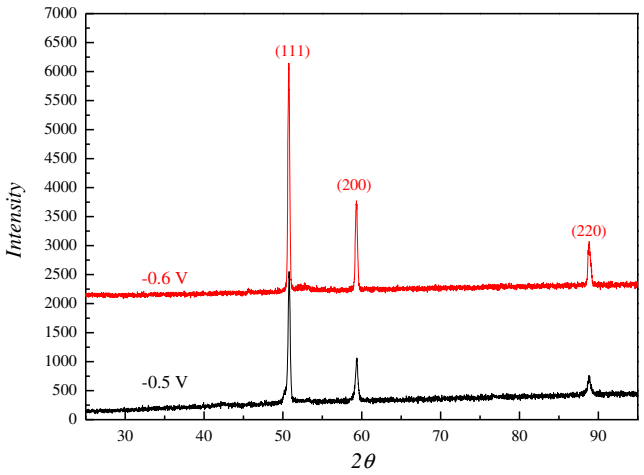

Fig. 13 XRD patterns of (Co K_α) of electrodeposited copper on mild steel from 0.025 M $Cu(TfO)_2$ in $[Py_{1,4}]TfO$ at 100 °C for 1 h

0.025 M $Cu(TfO)_2$ and 2.75 M $AlCl_3$ was prepared to study the deposition of copper aluminium alloys from $[Py_{1,4}]TfO$. All experiments were carried out at 100 °C. An appropriate quantity of $Cu(TfO)_2$ was added to $[Py_{1,4}]TfO$ and stirred to give a homogenous solution. To this solution, $AlCl_3$ was added slowly in small proportions and the mixture stirred to form a clear solution. Slowly the solution turned to a solid, which upon heating to 100 °C transformed to a clear and red coloured solution. Figure 14 shows four cyclic voltammograms of 0.025 M $Cu(TfO)_2$ and 2.75 M $AlCl_3$ in $[Py_{1,4}]TfO$ that were recorded at various switching potentials on gold at 100 °C. The working electrode potential was scanned from the open circuit potential to the negative direction. It is seen from Fig. 14 that the cyclic voltammograms exhibit two reduction waves at c_1 and c_2 and

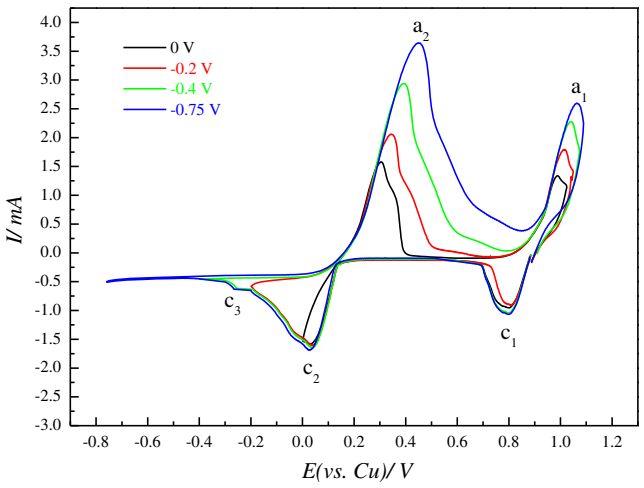

Fig. 14 Comparison of cyclic voltammograms of 0.025 M $Cu(TfO)_2$ and 2.75 M $AlCl_3$ in $[Py_{1,4}]TfO$ recorded at various switching potentials on gold at 100 °C. Scan rate=10 mVs^{-1}

the corresponding oxidation waves at a_1 and a_2, respectively. In addition, a third reduction wave was obtained at c_3 (~−0.3 V), and attributed either to the alloying of copper with aluminium or to the underpotential deposition of Al on growing Cu. The cathodic wave at c_1 is attributed to the reduction of Cu(II) to Cu(I) and its corresponding oxidation is observed at a_1. The bulk deposition of Cu was observed at c_2 and the corresponding stripping wave (at a_2) is observed upon scan reversal. The shoulders after the wave at c_2 might either be due to dissolution of Cu–Al alloy or due to the dissolution of Al UPD on Cu. There is no clear stripping peak during scan reversal, but we observed shoulders in the potential range of +0.3 to +0.6 V and these shoulders might be attributed to the dissolution of the deposited Cu–Al codeposits. This behaviour is in contrast to the behaviour that

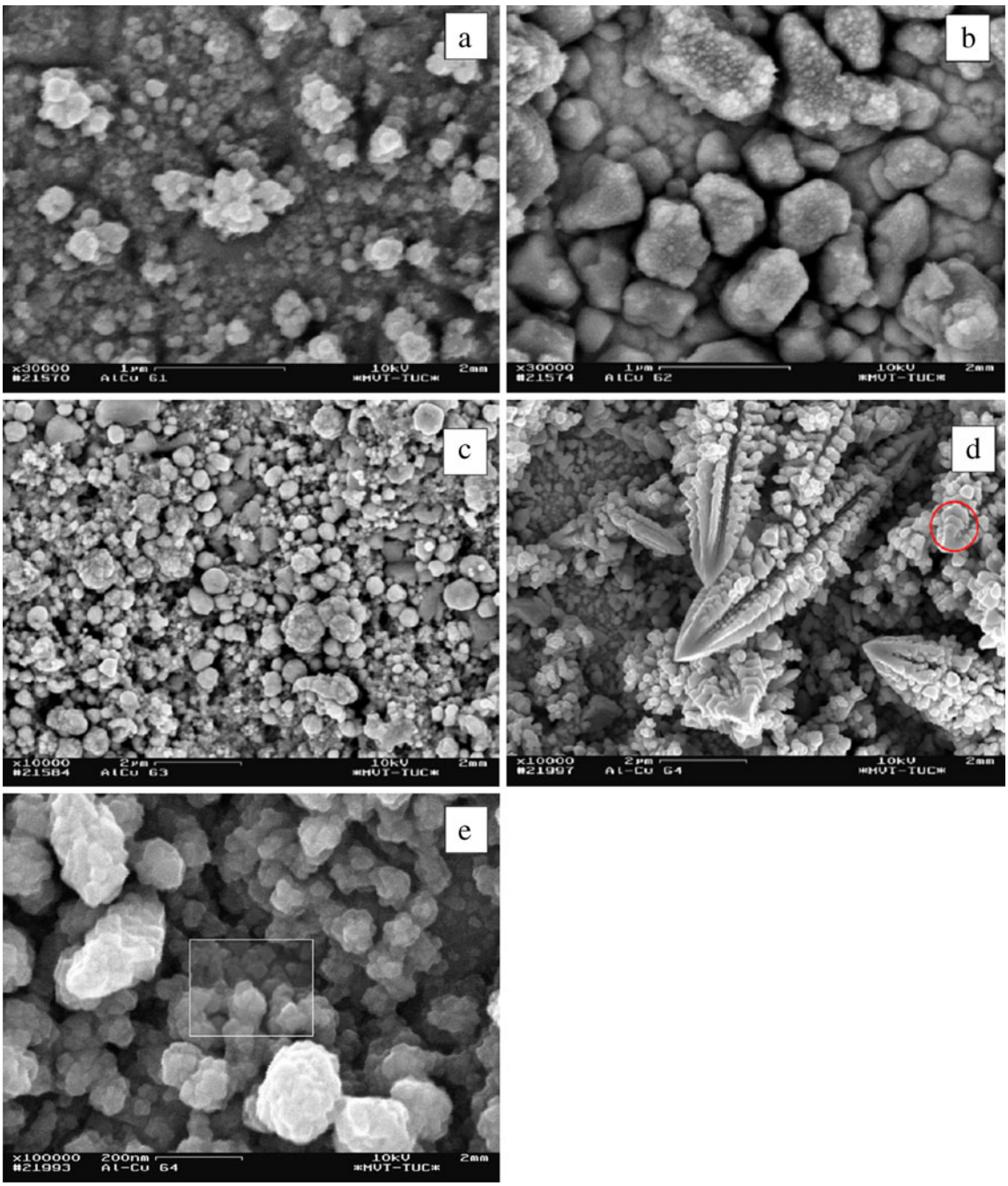

Fig. 15 **a–d** SEM micrographs of as deposited Cu–Al alloy on gold from 0.025 M $Cu(TfO)_2$ and 2.75 M $AlCl_3$ in $[Py_{1,4}]TfO$ at 100 °C. **a** −0.4 V, **b** −0.45 V, **c** −0.5 V, **d** −0.55 V. **e** SEM micrograph with higher magnification of a deposited Cu–Al alloy on gold from 0.025 M Cu $(TfO)_2$ and 2.75 M $AlCl_3$ in $[Py_{1,4}]TfO$ at −0.55 V at 100 °C

was observed in the case of [EMIm]Cl/$AlCl_3$ ionic liquids where oxidation waves were observed after the aluminium deposition [48].

Electrolysis was carried out at various applied deposition potentials (−0.40, −0.45, −0.5, and −0.55 V) to deposit Cu–Al alloys on gold from 0.025 M $Cu(TfO)_2$ and 2.75 M $AlCl_3$ in $[Py_{1,4}]TfO$. The obtained deposits were washed with isopropanol and water, then analysed by high-resolution SEM and XRD. The washed deposits were dissolved in a 1:1 HNO_3 HCl acid mixture to analyse the elemental composition of the alloy using AAS and ICPOES. A thick and uniform deposit was obtained with very fine crystal sizes (~60 nm) at −0.4 V and a particle size of 70 nm was obtained at −0.50 V. The corresponding high-resolution SEM images are shown in Fig. 15a–d. Agglomeration is also seen in the SEM images and the extent of agglomeration is increasing with decreasing electrode potential. In the case of a deposit obtained at −0.5 V, the deposit showed agglomerated fine structures (Fig. 15c). At a lower deposition potential (−0.55 V), needle-like structures are seen along with fine spherical structures (Fig. 15d).

Figure 15e shows the SEM micrograph with higher magnification of the Cu–Al deposit obtained from 0.025 M $Cu(TfO)_2$ and 2.75 M $AlCl_3$ in $[Py_{1,4}]TfO$ at −0.55 V on gold at 100 °C. It can be seen from the figure that nanostructures are observed with an average grain size of about 15 to 25 nm (see inset of Fig. 15e)

For XRD analysis, Cu–Al alloys were deposited on mild steel under the same conditions reported for gold. The XRD patterns of the electrodeposited copper–aluminium alloys from 0.025 M $Cu(TfO)_2$ and 2.75 M $AlCl_3$ in $[Py_{1,4}]TfO$ on mild steel at various applied potentials for 1 h are shown in Fig. 16. It can be seen that the deposited copper–aluminium alloy is crystalline and a strong diffraction peak (1210) is obtained along with the other characteristic diffraction peaks (111), (1012), (021), (202), (0022), (1216), and (234) (JCPDS no. 28-0005). Furthermore, the diffraction peaks are broad indicating the small crystallite size of Cu–Al deposit. The XRD patterns indicated that Cu_3Al deposit was obtained from the employed ionic liquid.

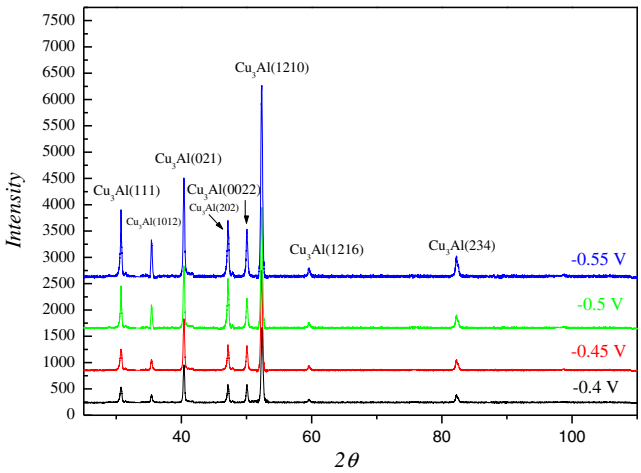

Fig. 16 XRD patterns of electrodeposited Cu–Al on mild steel at various applied potentials: *black line* −0.4 V, *red line* −0.45 V, *green line* −0.5 V, *blue line* −0.55 V

Summary and conclusions

From the above results, the following features can be summarised. The electrochemical window of the neat ionic liquid, $[Py_{1,4}]TfO$ was found to be ~5.75 and ~4.75 V at room temperature and 100 °C, respectively. A minimum concentration of 2.75 M $AlCl_3$ in $[Py_{1,4}]TfO$ is required to observe clearly bulk aluminium deposition. The electrochemical behaviour of aluminium species in $[Py_{1,4}]TfO$ is similar either on gold or on mild steel as concluded from the cyclic voltammograms. A nucleation loop was observed on both working electrodes. Thick and smooth layers of Al deposits were obtained. Nanocrystalline aluminium with an average grain size of 40 to 50 nm was obtained from the employed ionic liquid at 100 °C. Al deposition was also investigated from the ionic liquid [EMIm]TfO at 100 °C. The optimum concentration to obtain bulk Al deposits from [EMIm]TfO was found to be 4.6 M $AlCl_3$. Al can only be deposited from the upper phase of biphasic mixture of 4.6 M $AlCl_3$ in [EMIm]TfO. The onset of bulk Al deposition was found to be at −0.1 V (vs. Al) from [EMIm]TfO/$AlCl_3$. Al is obtained as a microcrystalline material.

The cyclic voltammogram of 0.01 M $Cu(TfO)_2$ in $[Py_{1,4}]TfO$ shows two reduction and two oxidation waves. The two reduction and oxidation waves were attributed to the reduction of Cu(II) to Cu(I) and Cu(I) to metallic copper and Cu to Cu(I) and Cu(I) to Cu(II), respectively. Nanocrystalline copper deposits were obtained by constant potential electrolysis. The average grain size of the copper deposit was found to be between 20 and 40 nm.

The cyclic voltammograms of 0.025 M $Cu(TfO)_2$ and 2.75 M $AlCl_3$ in $[Py_{1,4}]TfO$ exhibited two reduction and oxidation waves corresponding to the reduction of Cu(II) to Cu(I) and Cu(I) to metallic copper, respectively. Aluminium codeposition or underpotential deposition of Al on growing Cu was found to occur at around −0.3 V in the cyclic voltammograms. This behaviour is different from the behaviour that is observed in acidic chloroaluminate ionic liquid systems. The morphology of the Cu–Al alloys depends on the deposition potentials. SEM micrographs revealed that nanocrystalline structures of copper–aluminium deposits were obtained from the electrolysis experiments and the average grain size was found to be between 60 and 70 nm. The average grain size of the deposit was significantly decreased to ~15 to 25 nm at lower deposition potentials. XRD analysis indicated that

Cu_3Al alloy was formed. It can be concluded that nanocrystalline Cu–Al alloys can be obtained from ionic liquids with the pyrrolidinium cation.

References

1. Hurley FH, Weir TP Jr (1951) J Electrochem Soc 98:203–206
2. Hurley FH, Weir TP Jr (1951) J Electrochem Soc 98:207–212
3. Robinson J, Osteryoung RA (1980) J Electrochem Soc 127:122–128
4. Welch BJ, Osteryoung RA (1981) J Electroanal Chem 118:455–466
5. Lipsztajn M, Osteryoung RA (1983) J Electrochem Soc 130:1968–1969
6. Lai PK, Skyllas-Kazacos M (1987) Electrochim Acta 32:1443–1449
7. Melton TJ, Joyce V, Maloy JT, Boon JA, Wilkes JS (1990) J Electrochem Soc 137:3865–3869
8. Carlin RT, Crawford W, Bersch M (1992) J Electrochem Soc 139:2720–2727
9. Moffat TP, Stafford GR, Hall DE (1993) J Electrochem Soc 140:2779–2786
10. Yang C-C (1994) Mater Chem Phys 37:355–361
11. Liao Q, Pitner WR, Stewart G, Hussey CL, Stafford GR (1997) J Electrochem Soc 144:936–943
12. Zhao Y, VanderNoot T (1997) J Electrochim Acta 42:3–13
13. Zhao Y, VanderNoot T (1997) J Electrochim Acta 42:1639–1643
14. Tsuda T, Hussey CL, Stafford GR, Bonevich V (2003) J Electrochem Soc 150:C234–C243
15. Tsuda T, Hussey CL, Stafford GR (2004) J Electrochem Soc 151:C379–C384
16. Jiang T, Chollier Brym MJ, Dubé G, Lasia A, Brisard GM (2006) Surf Coat Technol 201:1–9
17. Jiang T, Chollier Brym MJ, Dubé G, Lasia A, Brisard GM (2006) Surf Coat Technol 201:10–18
18. Liu QX, Zein El Abedin S, Endres F (2006) Surf Coat Technol 201:1352–1356
19. Yue G, Zhang S, Zhu Y, Lu X, Li S, Li Z (2009) AICHE J 55:783–796
20. Zein El Abedin S, Moustafa EM, Hempelmann R, Natter H, Endres F (2006) Chem Phys Chem 7:1535–1543
21. Cervera SJL, König A (2010) Chem Eng Technol 33:1979–1988
22. Atkin R, Zein El Abedin S, Hayes R, Gasparotto LHS, Borisenko N, Endres F (2009) J Phys ChemC 113:13266–13272
23. Liu QX, Zein El Abedin S, Endres F (2008) J Electrochem Soc 155:D357–D362
24. Zein El Abedin S, Giridhar P, Schwab P, Endres F (2010) Electrochem Commun 12:1084–1086
25. Ismail AS, Zein El Abedin S, Höfft O, Endres F (2010) Electrochem Comm 12:909–911
26. Gewirth AA, Andricacos PC, Switzer JA, Dukovic JO (1998) Electrochem Soc Interface 7:1–4
27. Andricacos PC (1999) Electrochem Soc Interface 8:32–37
28. Hussey CL, King LA, Carpio RA (1979) J Electrochem Soc 126:1029–1034
29. Nanjundiah C, Osteryoung RA (1983) J Electrochem Soc 130:1312–1318
30. Schweizer A, Endres F (2000) Phys Chem Chem Phys 2:5455–5462
31. Chen PY, Sun IW (1999) Electrochim Acta 45:441–450
32. Yu L, Sun H, He J, Wang D, Jin X, Hu X, Chen GZ (2007) Electrochem Comm 9:1374–1381
33. Leong TI, Sun IW, Deng MJ, Wu CM, Chen PY (2008) J Electrochem Soc 155:F55–F60
34. Zein El Abedin S, Pölleth M, Meiss SA, Janek J, Endres F (2007) Green Chemistry 9:549–553
35. Murase K, Nitta K, Hirato T, Awakura Y (2001) J App Electrochem 31:1089–1094
36. Katase T, Murase K, Hirato T, Awakura Y (2007) J App Electrochem 37:339–344
37. Zein El Abedin S, Saad AY, Farag HK, Borisenko N, Liu QX, Endres F (2007) Electrochim Acta 52:2746–2754
38. Abbott AP, Ttaib KE, Frisch G, McKenzie KJ, Ryder KS (2009) Phys Chem Chem Phys 11:4269–4277
39. Nicol MJ, Philip HI (1976) J Electroanal Chem 70:233–237
40. Moffat TP (1994) J Electrochem Soc 141:3059–3070
41. Stafford GR (1989) J Electrochem Soc 136:635–369
42. Stafford GR (1994) J Electrochem Soc 141:945–953
43. Zhu Q, Hussey CL, Stafford GR (2001) J Electrochem Soc 148:C88–C94
44. Pitner WR, Hussey CL, Stafford GR (1996) J Electrochem Soc 143:130–138
45. Ali MR, Nishikata A, Tsuru T (1997) Electrochim Acta 42:1819–1828
46. Carlin RT, Trulove PC, De Long HC (1996) J Electrochem Soc 143:2747–2758
47. Mitchell JA, Pitner WR, Hussey CL, Stafford GR (1996) J Electrochem Soc 143:3448–3455
48. Tierney BJ, Pitner WR, Mitchell JA, Hussey CL, Stafford GR (1998) J Electrochem Soc 145:3110–3116
49. Zhu Q, Hussey CL (2001) J Electrochem Soc 148:C395–C402
50. Eiden P, Liu Q, Zein El Abedin S, Endres F, Krossing I (2009) Chem Eur J 15:3426–3434
51. Rocher NM, Izgorodina EI, Rüther T, Forsyth M, MacFarlane DR, Rodopoulos T, Horne MD, Bond AM (2009) Chem Eur J 15:3435–3447
52. Rodopoulos T, Smith L, Horne MD, Rüther T (2010) Chem Eur J 16:3815–3826
53. Giridhar P, Zein El Abedin S, Endres F (2012) Electrochim Acta 70:210–214
54. Scherrer P (1918) Göttinger Nachrichten 2:98
55. Kroon MC, Buijs W, Peters Cor J, Witkamp Geert-Jan (2006) Green Chem 8:241–245